



**HAL**  
open science

## Structural Science Experimental charge density and electrostatic potential of glycyl-L-threonine dihydrate

Farid Benabicha, Virginie Pichon-Pesme, Christian Jelsch, Claude Lecomte,  
Ahmed Khmou

► **To cite this version:**

Farid Benabicha, Virginie Pichon-Pesme, Christian Jelsch, Claude Lecomte, Ahmed Khmou. Structural Science Experimental charge density and electrostatic potential of glycyl-L-threonine dihydrate. Acta Crystallographica Section B: Structural Science, Crystal Engineering and Materials [2014-..], 2000, B56, pp.155-165. 10.1107/s0108768199014251 . hal-01713030

**HAL Id: hal-01713030**

**<https://hal.science/hal-01713030>**

Submitted on 20 Feb 2018

**HAL** is a multi-disciplinary open access archive for the deposit and dissemination of scientific research documents, whether they are published or not. The documents may come from teaching and research institutions in France or abroad, or from public or private research centers.

L'archive ouverte pluridisciplinaire **HAL**, est destinée au dépôt et à la diffusion de documents scientifiques de niveau recherche, publiés ou non, émanant des établissements d'enseignement et de recherche français ou étrangers, des laboratoires publics ou privés.

# Experimental charge density and electrostatic potential of glycyl-L-threonine dihydrate

Farid Benabicha,<sup>a,b</sup> Virginie Pichon-Pesme,<sup>a</sup> Christian Jelsch,<sup>a</sup> Claude Lecomte<sup>a\*</sup> and Ahmed Khmou<sup>b</sup>

<sup>a</sup>LCM3B, Laboratoire de Cristallographie et Modélisation des Matériaux Minéraux et Biologiques, Université Henri Poincaré-Nancy 1, UPRES A CNRS 7036, Faculté des Sciences, BP 239, 54506 Vandoeuvre les Nancy CEDEX, France, and <sup>b</sup>Département de Physique, Université Moulay Ismail, Faculté des Sciences, Meknès, Morocco

Correspondence e-mail:  
lecomte@lcm3b.u-nancy.fr

The experimental electron density distribution in glycyl-L-threonine dihydrate has been investigated using single-crystal X-ray diffraction data at 110 K to a resolution of  $(\sin \theta/\lambda) = 1.2 \text{ \AA}^{-1}$ . Multipolar pseudo-atom refinement was carried out against 5417 observed data and the molecular electron density was analyzed using topological methods. The experimental electrostatic potential around the molecule is discussed in terms of molecular interactions. Crystal data:  $\text{C}_6\text{H}_{12}\text{N}_2\text{O}_4 \cdot 2\text{H}_2\text{O}$ ,  $M_r = 212.2$ , orthorhombic,  $P2_12_12_1$ ,  $Z = 4$ ,  $F(000) = 456 \text{ e}$ ,  $T = 110 \text{ K}$ ,  $a = 9.572(3)$ ,  $b = 10.039(3)$ ,  $c = 10.548(2) \text{ \AA}$ ,  $V = 1013.6(4) \text{ \AA}^3$ ,  $D_x = 1.3 \text{ g cm}^{-3}$ ,  $\mu = 1.2 \text{ cm}^{-1}$  for  $\lambda_{\text{Mo}} = 0.7107 \text{ \AA}$ .

Received 28 May 1999

Accepted 4 November 1999

## 1. Introduction

We have been involved for many years in the ultra high-resolution X-ray diffraction of peptides and amino acids (Souhassou *et al.*, 1991, 1992; Pichon-Pesme *et al.*, 1992; Pichon-Pesme & Lecomte, 1998; Wiest *et al.*, 1994; Dahaoui, Pichon-Pesme *et al.*, 1999). In these studies, we have described the atomic electron density with the most frequently used multipole formalism (Hansen & Coppens, 1978). These studies allowed us to show that the pseudo-atom aspherical scattering factors obtained can be transferable from one molecule to another (Pichon-Pesme *et al.*, 1995). This transferability permits a more precise definition of the atomic scattering factors for any atom in a given chemical state and environment. Therefore, we decided to build a database of charge density parameters for atom types found in proteins (Housset *et al.*, 2000). This will enable us to refine ultra-high-resolution small protein structures using charged multipolar atoms to accurately describe the molecular electron density distribution (Jelsch *et al.*, 1998). To complement our databank we report here on the electron density distribution of glycyl-L-threonine dihydrate, for which a room-temperature crystal structure was first reported by Yadava & Padmanabhan (1973). Besides the electron density, topological properties and the electrostatic potential of the charge density will also be discussed.

## 2. Crystallographic analysis

### 2.1. Data collection

Glycyl-L-threonine (GlyThr) was crystallized from water by solvent evaporation. A crystal of dimensions  $0.3 \times 0.3 \times 0.15 \text{ mm}$  was used to collect low-temperature Mo  $K\alpha$  X-ray diffraction data on an Enraf-Nonius CAD-4F diffractometer equipped with a nitrogen-vapor stream device and installed in a dry-box to prevent ice formation on the crystal. The gas

**Table 1**

Experimental details.

Crystal data	
Chemical formula	C <sub>6</sub> H <sub>12</sub> N <sub>2</sub> O <sub>4</sub> ·2(H <sub>2</sub> O)
Chemical formula weight	212.21
Cell setting	Orthorhombic
Space group	<i>P</i> 2 <sub>1</sub> 2 <sub>1</sub> 2 <sub>1</sub>
<i>a</i> (Å)	9.572 (3)
<i>b</i> (Å)	10.039 (3)
<i>c</i> (Å)	10.548 (3)
<i>V</i> (Å <sup>3</sup> )	1013.7 (5)
<i>Z</i>	4
<i>D<sub>x</sub></i> (Mg m <sup>-3</sup> )	1.390
Radiation type	Mo <i>K</i> α
Wavelength (Å)	0.71068
No. of reflections for cell parameters	25
$\theta$ range (°)	11–20
$\mu$ (mm <sup>-1</sup> )	0.124
Temperature (K)	110 (5)
Crystal form	Rectangular prism
Crystal size (mm)	0.30 × 0.30 × 0.15
Crystal color	Colorless
Data collection	
Diffraction method	Enraf–Nonius CAD-4
Data collection method	$\omega/2\theta$ scans
Absorption correction	None
No. of measured reflections	15 903
No. of independent reflections	5417
No. of observed reflections	3978
Criterion for observed reflections	<i>I</i> > 3σ( <i>I</i> )
<i>R<sub>int</sub></i>	0.0233
$\theta_{\max}$ (°)	54.91
Range of <i>h, k, l</i>	–22 → <i>h</i> → 22 –23 → <i>k</i> → 23 0 → <i>l</i> → 24
No. of standard reflections	4
Frequency of standard reflections	Every 120 min
Intensity decay (%)	3
Refinement	
Refinement on	<i>F</i>
<i>R</i>	0.0247
No. of reflections used in refinement	3978
No. of parameters used	405
H-atom treatment	Only H-atom <i>U</i> 's refined
Weighting scheme	$w = 1/[\sigma^2(F_o^2)]$
( $\Delta/\sigma$ ) <sub>max</sub>	0.05
$\Delta\rho_{\max}$ (e Å <sup>-3</sup> )	0.10
$\Delta\rho_{\min}$ (e Å <sup>-3</sup> )	–0.10
Extinction method	None
Source of atomic scattering factors	Clementi & Raimondi (1963)
Computer programs	
Data collection	CAD-4 (Enraf–Nonius, 1989)
Cell refinement	CAD-4 (Enraf–Nonius, 1989)
Data reduction	DREAR (Blessing, 1987, 1989)
Structure solution	SHELXS–97 (Sheldrick, 1990)
Structure refinement	MOLLY (Hansen & Coppens, 1978)

stream temperature was maintained at 110 ± 5 K, as monitored by a copper-constantan thermocouple positioned ~5 cm upstream from the crystal. Lattice parameters were obtained by least-squares fit to the optimized setting angles of the *K*α<sub>1</sub> peaks of 25 reflections with 22 < 2θ < 40°. Intensity data were recorded as ω–2θ scan profiles to a resolution of (sin θ/λ)<sub>max</sub> = 1.2 Å<sup>-1</sup> for a total of 15 903 reflections in the following way:

for reflections with sin θ/λ < 0.9 Å<sup>-1</sup>, four equivalent sets of reflections in the Laue group *mmm* (*hkl*,  $\bar{h}kl$ ,  $h\bar{k}l$ ,  $hkl$ ) were collected and only two (*hkl*,  $\bar{h}kl$ ) for 0.9 < sin θ/λ < 1.2 Å<sup>-1</sup> when the intensity was estimated to be significant. This was determined by a previous calculation of structure factors from the initial structure. During the data collection, four standard reflections ( $\bar{5}44$ , 251, 033 and 073) were measured at 2 h intervals. The total scan width (Δω) was (1.00 + 0.35tan θ)°, with a constant detector aperture of 6 × 4 mm<sup>2</sup>. The scan speed depending on the signal-to-noise ratio in the range 0.63–2.75° min<sup>-1</sup> was used for the low-angle data collection (sin θ/λ < 0.9 Å<sup>-1</sup>). The high-angle data were recorded with a constant scan speed (0.63° min<sup>-1</sup>). The total exposure time was 482 h; no crystal, temperature or diffractometer problems occurred. Full experimental details are given in Table 1.

## 2.2. Data processing

Data reduction and error analysis were performed using DREAR (Blessing, 1987, 1989) programs. Reflection integration limits were taken from a Lorentzian model for peak-width variations. A polynomial fit to the smooth decline of ~3% in the standard reflection intensities over X-ray exposure was used to scale the data and to derive the instrumental instability coefficient *p* = 0.019 used in the estimation of the experimental intensity variances σ<sup>2</sup>(*I*<sup>2</sup>) = σ<sub>c</sub><sup>2</sup>(*I*<sup>2</sup>) + (*pI*<sup>2</sup>)<sup>2</sup>, where σ<sub>c</sub><sup>2</sup> are counting statistics errors. No absorption correction was performed. Averaging equivalent measurements led to 5417 unique reflections (*I* > 0), of which 3978 had *I* > 3 σ(*I*). The internal agreement indices, defined as  $R = \sum ||F|^2 - \langle |F|^2 \rangle| / \sum |F|^2$  and  $wR = [\sum w (|F|^2 - \langle |F|^2 \rangle) / \sum w |F|^2]^{1/2}$ , *w* = 1/σ<sup>2</sup>(*I*<sup>2</sup>), were *R* = 0.023 and *wR* = 0.052 for all data, and 0.020 and 0.021 for the 642 data with sin θ/λ < 0.5 Å<sup>-1</sup>.

## 2.3. Least-squares refinements

The crystal structure at room temperature was determined by Yadava & Padmanabhan (1973) from Weissenberg data. The present low-temperature structure was solved by SHELXS86 (Sheldrick, 1990); all H atoms were found by Fourier difference synthesis and refined initially using SHELXL (Sheldrick, 1993)

The least-squares program MOLLY (Hansen & Coppens, 1978) was used to determine atomic coordinates, thermal displacement parameters and multipolar density coefficients. The bound-atom form factor for the hydrogen from Stewart *et al.* (1965), the calculated form factor for the non-H atoms from Clementi & Raimondi (1963) wave functions, and the real and imaginary dispersion corrections to the form factor given by Cromer (1974) were used in the structure factor calculations. In the model of Hansen & Coppens (1978) the electron density of the unit cell is described as the superposition of pseudo-atomic electron densities

$$\rho(\mathbf{r}) = \rho_{\text{core}}(r) + P_{\text{val}}k^3\rho_{\text{val}}(kr) + \sum_{l=0}^{l_{\text{max}}} k^3 R_{nl}(k'r) \sum_{m=0}^l P_{lm}y_{lm\pm}(\theta, \varphi), \quad (1)$$

**Table 2**

Statistics of the least-squares refinements.

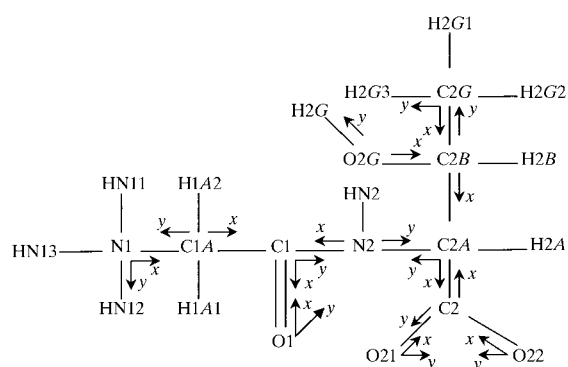
$s = \sin \theta/\lambda$ ;  $R = \sum(K|F_o| - |F_c|/\sum|F_o|)$ ;  $wR = (\chi^2/\sum w|F_o|^2)^{1/2}$ ;  $\chi^2 = \sum w(|F_o| - K|F_c|)^2$ ;  $w = 1/\sigma^2(|F_o|)$ ;  $S = [\chi^2/(n_{\text{obs}} - n_{\text{var}})]^{1/2}$  goodness of fit;  $n_{\text{obs}}$  number of reflections,  $n_{\text{var}}$  number of varied parameters.

Refinement	Type of refinement	$s$ ( $\text{\AA}^{-1}$ )	$R$	$wR$	$S$	Scale factor	$n_{\text{var}}$	$n_{\text{obs}}$
<i>A</i>	Spherical	$0.9 < s < 1.2$	0.0458	0.0481	0.78	0.693	127	1153
<i>B</i>	Spherical	$s < 0.9$	0.0372	0.0462	2.08	0.708	65	2825
<i>C</i>	Multipolar	$s < 1.2$	0.0301	0.0314	1.21	0.698	148	3978
<i>D</i>	Multipolar	$s < 1.2$	0.0247	0.0233	0.93	0.710	405	3978
<i>E</i>	Kappa	$s < 1.2$	0.0348	0.0402	1.55	0.708	61	3978

where  $\rho_{\text{core}}$  and  $\rho_{\text{val}}$  are Hartree–Fock spherical core and valence densities, respectively. In this aspherical density model, the refined valence population parameter  $P_{\text{val}}$  gives an estimation of the net atomic charge  $q$  with respect to the number of valence electrons  $N_{\text{val}}$  in the free atom:  $q = N_{\text{val}} - P_{\text{val}}$ . The  $y_{\text{lm}\pm}$ s are spherical harmonic angular functions of the order  $l$  in real form and  $R_{n_l}(r)$  are Slater-type radial functions. The  $P_{\text{lm}}$ s are the multipolar population parameters of each associated spherical harmonic  $y_{\text{lm}\pm}$ , and  $\kappa$  and  $\kappa'$  are the contraction–expansion coefficients (Coppens *et al.*, 1979) for the spherical and multipolar valence densities, respectively. Fig. 1 gives the atomic numbering schemes and local coordinate system used in the multipolar refinement for the GlyThr molecule. The different steps of the refinement and reliability indices are given in Table 2.

At first, the positional  $xyz$  parameters and anisotropic displacement parameters of the non-H atoms were refined against high-order data with  $(\sin \theta/\lambda) > 0.9 \text{ \AA}^{-1}$  (refinement *A*). Then the positional and isotropic displacement parameters of the H atoms were refined against low-order data with  $(\sin \theta/\lambda) < 0.9 \text{ \AA}^{-1}$  (refinement *B*). The coordinates of the H atoms were adjusted by extension along the  $\text{Csp}^3\text{—H}$ ,  $\text{N—H}$ ,  $\text{O—H}$  and  $\text{Ow—H}$  axes (Ow is the oxygen of the water molecule), respectively, to 1.083, 1.032, 0.964 and 0.960  $\text{\AA}$  bond lengths, which are the average values from neutron diffraction (Allen, 1986).

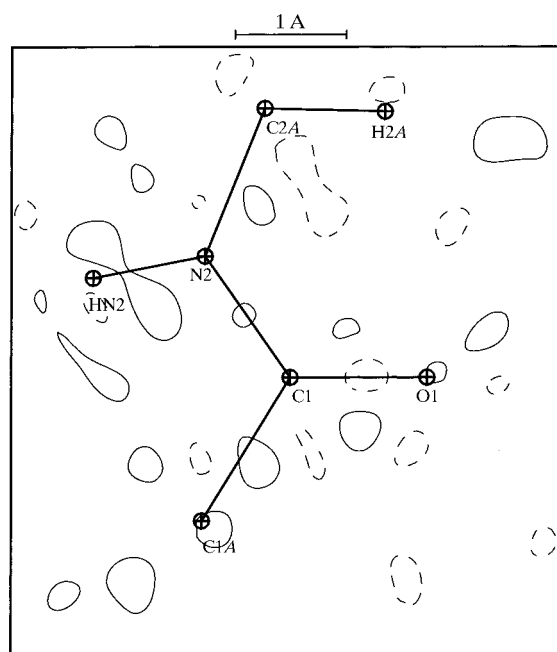
Symmetry and chemical constraints were applied to the non-H atoms at the beginning of the multipolar refinement (refinement *C* in Table 2) in order to reduce the number of variables. The C, O and N atoms, those of the carboxyl groups and those of water molecules, were constrained to be planar.

**Figure 1**

Atomic numbering scheme and local coordinates system for GlyThr.

Five types of H atoms were defined: H (C) linked to  $\text{Csp}^3$ , H (N1) for the  $\text{NH}_3^+$  group, H (N2) for the peptide NH, H (O) for the threonine side-chain and H (Ow) linked to the water O atoms. For all H atoms only one dipole along the  $X\text{—H}$  bond ( $X = \text{C}, \text{O}, \text{N}$ ) was refined, whereas multipoles up to  $l = 3$  (octupole level) were used for the non-H atoms. During the multipolar refinement, the  $P_v$  parameters were constrained in order to keep the GlyThr and water molecules neutral. The strategy of refinement *C* was as follows: with fixed  $xyz$ ,  $U^{ij}$  values taken from refinement *A* for the non-H atoms and refinement *B* for H atoms,  $P_v + \text{scale}$ , then  $P_{\text{lm}} + \text{scale}$ ,  $\kappa + \text{scale}$  and finally  $\kappa' + \text{scale}$ . This process was recycled until convergence.

In refinement *D* all chemical constraints were released progressively. The refinement strategy was the same as in refinement *C*; then,  $xyz$ ,  $U^{ij}$  of the non-H atoms and the isotropic displacement parameters of the H atoms were refined. Finally, the  $U^{ij}$  of the non-H atoms and all  $P_{\text{lm}}$  were refined together. No extinction refinement was deemed necessary. In this refinement (*D*), the crystallographic agree-

**Figure 2**

Residual electron density in the C1, O1 and N2 plane of the peptide bond (after refinement *D*). Contour intervals are at  $0.05 \text{ e \AA}^{-3}$ ; solid lines represent positive contours, dashed lines negative contours and zero contours are omitted.

**Table 3**

Fractional atomic coordinates and equivalent isotropic displacement parameters ( $\text{\AA}^2$ ) from refinement *D*.

The form of the temperature factor for non-H atoms is  $T = \exp(-2\pi^2 \sum_i \sum_j h_i h_j a_i^* a_j^* U^{ij})$ .

	<i>x</i>	<i>y</i>	<i>z</i>	$U_{\text{eq}}/U_{\text{iso}}$
HN11	0.29923	-0.48326	0.58126	0.017 (3)
HN12	0.14652	-0.51721	0.67651	0.019 (3)
HN13	0.2388	-0.39164	0.69861	0.017 (3)
H2A	0.23901	-0.01902	0.41133	0.015 (2)
H2G1	0.19334	-0.24265	0.22270	0.033 (3)
H2G2	0.32464	-0.12909	0.20171	0.033 (3)
H2G3	0.19853	-0.13968	0.07895	0.033 (3)
H1A1	0.09721	-0.44392	0.45777	0.016 (2)
H1A2	0.01796	-0.34659	0.58629	0.017 (2)
HN2	-0.01183	-0.19992	0.44081	0.015 (2)
H2B	0.14321	0.0573	0.21284	0.019 (3)
H2G	-0.04333	-0.15493	0.16731	0.016 (3)
Hw11	-0.12677	0.18846	0.60235	0.023 (2)
Hw12	-0.243	0.27697	0.63945	0.028 (2)
Hw21	-0.03766	0.34145	0.73715	0.041 (3)
Hw22	0.02516	0.43039	0.84732	0.033 (3)

	<i>x</i>	<i>y</i>	<i>z</i>	$U_{11}$	$U_{22}$	$U_{33}$	$U_{12}$	$U_{13}$	$U_{23}$
C1A	0.11292 (5)	-0.38015 (5)	0.53973 (5)	0.0102 (2)	0.0104 (2)	0.0163 (3)	-0.0014 (1)	-0.0026 (2)	0.0020 (2)
C1	0.17857 (5)	-0.24934 (5)	0.49970 (4)	0.0079 (2)	0.0099 (1)	0.0116 (2)	0.0002 (2)	-0.0004 (1)	0.0009 (1)
C2A	0.13187 (5)	-0.04093 (5)	0.38561 (4)	0.0088 (2)	0.0103 (2)	0.0123 (2)	-0.0006 (2)	0.0000 (2)	0.0012 (2)
C2B	0.11723 (6)	-0.04410 (6)	0.24045 (5)	0.0153 (2)	0.0151 (2)	0.0116 (2)	-0.0029 (2)	0.0019 (2)	0.0007 (2)
C2G	0.21530 (7)	-0.14443 (7)	0.18052 (6)	0.0178 (3)	0.0326 (4)	0.0216 (3)	0.0010 (3)	0.0066 (3)	-0.0082 (3)
C2	0.04583 (5)	0.07540 (5)	0.43915 (5)	0.0093 (2)	0.0097 (2)	0.0131 (2)	-0.0004 (1)	-0.0012 (2)	0.0008 (1)
O1	0.30234 (4)	-0.22458 (4)	0.52137 (4)	0.0088 (2)	0.0149 (2)	0.0223 (3)	-0.0016 (2)	-0.0025 (2)	0.0055 (2)
O2G	-0.02571 (4)	-0.07192 (4)	0.21065 (4)	0.0157 (2)	0.0144 (2)	0.0147 (2)	0.0011 (2)	-0.0030 (2)	-0.0019 (2)
O21	-0.05779 (4)	0.04844 (4)	0.50909 (3)	0.0115 (1)	0.0136 (2)	0.0155 (2)	-0.0002 (1)	0.0024 (2)	-0.0008 (1)
O22	0.08373 (4)	0.18971 (4)	0.40860 (4)	0.0145 (2)	0.0095 (2)	0.0260 (2)	-0.0004 (2)	0.0009 (3)	0.0040 (2)
N1	0.20802 (5)	-0.45253 (4)	0.62489 (4)	0.0112 (2)	0.0119 (2)	0.0143 (2)	0.0001 (2)	-0.0011 (2)	0.0028 (2)
N2	0.09031 (4)	-0.16725 (4)	0.43985 (4)	0.0083 (2)	0.0099 (2)	0.0153 (2)	0.0001 (2)	-0.0010 (2)	0.0027 (2)
Ow1	-0.16550 (4)	0.23049 (4)	0.67630 (4)	0.0157 (2)	0.0179 (2)	0.0162 (2)	0.0026 (2)	0.0003 (2)	-0.0023 (2)
Ow2	0.04059 (6)	0.39211 (5)	0.76544 (5)	0.0422 (4)	0.0389 (4)	0.0202 (3)	-0.0268 (4)	0.0134 (3)	-0.0091 (3)

ment factors improve significantly. At last, the atomic net charges, fundamental for the determination of electrostatic properties or of force fields for molecular modeling, were determined from a kappa refinement (Coppens *et al.*, 1979; refinement *E* in Table 2) with *xyz* and  $U^{ij}$  parameters from refinement *D*.

Table 3 lists the fractional coordinates and the final atomic anisotropic displacement amplitudes obtained after refinement *D*. The Hirshfeld rigid-bond test (Hirshfeld, 1976) was carried out in order to check the atomic thermal displacement parameters. All mean-square displacement amplitudes along bond directions differed by less than  $0.001 \text{\AA}^2$ , indicating that the multipole refinement yielded an effective deconvolution of the mean-square displacements from the valence electron density deformation. The electron density parameters from multipolar refinement *D* are given in the supplementary material.<sup>1</sup> Fig. 2 shows the final residual density map after refinement *D* [ $\sin \theta/\lambda = 0.9 \text{\AA}^{-1}$ ,  $I > 3\sigma(I)$ ] in the plane of the peptide bond: the maximum and minimum densities do not exceed  $\pm 0.05 \text{ e \AA}^{-3}$ , in accordance with the estimates of the

<sup>1</sup>Supplementary data for this paper are available from the IUCr electronic archives (Reference: AN0564). Services for accessing these data are described at the back of the journal.

**Table 4**

Torsion angles in GlyThr.

The standard uncertainties are given in parentheses.

Bond	Atoms	Designation	Angle ( $^\circ$ )
$C_\alpha-C'$	N1-C1A-C1-N2	$\psi_{11}$	-169.30 (4)
	N1-C1A-C1-O1	$\psi_{12}$	11.01 (6)
$C'-N$	C1A-C1-N2-C2A	$\omega$	-175.72 (5)
$N-C_\alpha$	C1-N2-C2A-C2	$\varphi_{21}$	-123.48 (5)
	C1-N2-C2A-C2B	$\varphi_{22}$	114.26 (5)
$C_\alpha-C'$	N2-C2A-C2-O22	$\psi_T^1$	172.52 (4)
	N2-C2A-C2-O21	$\psi_T^2$	-8.15 (6)
$C_\alpha-C_\beta$	N2-C2A-C2B-C2G	$\chi_{21}$	-64.23 (5)
	N2-C2A-C2B-O2G	$\chi_{22}$	59.23 (5)

average error in the experimental difference density maps (Cruickshank, 1949; Rees, 1976)

$$\langle \sigma^2(\Delta\rho) \rangle^{1/2} = (2/V)[\Sigma(\sigma^2|F_o|)]^{1/2} = 0.04 \text{ e \AA}^{-3} \quad (2)$$

and

$$\begin{aligned} \langle \sigma^2(\Delta\rho) \rangle^{1/2} &= (2/V)[\Sigma(K^{-1}|F_o| - |F_m|)^2]^{1/2} \\ &= 0.04 \text{ e \AA}^{-3}, \end{aligned} \quad (3)$$

**Table 5**  
Selected geometric parameters ( $\text{\AA}^2$ ,  $^\circ$ ).

C1—O1	1.2319 (6)	C1A—N1	1.4709 (6)
C2—O22	1.2459 (6)	C2B—C2G	1.5151 (8)
C2—O21	1.2655 (6)	C1—C1A	1.5159 (7)
C2B—O2G	1.4314 (6)	C2—C2A	1.5366 (7)
C1—N2	1.3385 (6)	C2A—C2B	1.5381 (7)
C2A—N2	1.4470 (6)		
N1—C1A—C1	109.97 (4)	C2—C2A—C2B	109.44 (4)
C1A—C1—O1	121.46 (4)	O2G—C2B—C2G	111.77 (4)
C1A—C1—N2	113.76 (4)	O2G—C2B—C2A	108.05 (4)
O1—C1—N2	124.77 (4)	C2G—C2B—C2A	111.89 (5)
C1—N2—C2A	123.55 (4)	C2A—C2—O21	118.15 (4)
N2—C2A—C2B	110.52 (4)	C2A—C2—O22	116.67 (4)
N2—C2A—C2	111.92 (4)	O22—C2—O21	125.17 (5)

**Table 6**  
Hydrogen-bonding geometry ( $\text{\AA}$ ,  $^\circ$ ) from GlyThr.

The standard uncertainties (s.u.s), estimated from the non-H atom s.u.s, are given in parentheses.

$D-H \cdots A$	$D-H$	$H \cdots A$	$D \cdots A$	$D-H \cdots A$
N1—HN11 $\cdots$ O21 <sup>i</sup>	1.0338 (7)	1.7915 (4)	2.8195 (6)	172.20 (3)
N1—HN12 $\cdots$ Ow2 <sup>ii</sup>	1.0321 (6)	1.6544 (5)	2.6832 (6)	174.39 (3)
N1—HN13 $\cdots$ Ow1 <sup>iii</sup>	1.0325 (7)	1.9331 (4)	2.8178 (6)	141.85 (3)
N2—HN2 $\cdots$ O1 <sup>iv</sup>	1.0312 (6)	1.9742 (3)	2.9907 (5)	168.03 (2)
O2G—H2G $\cdots$ O22 <sup>v</sup>	0.9662 (8)	1.7954 (4)	2.7600 (5)	177.17 (4)
Ow1—Hw11 $\cdots$ O21	0.9591 (7)	1.8384 (4)	2.7413 (5)	155.29 (3)
Ow1—Hw12 $\cdots$ O22 <sup>vi</sup>	0.9613 (7)	1.7662 (4)	2.6843 (6)	159.25 (2)
Ow2—Hw21 $\cdots$ Ow1	0.9537 (8)	1.7749 (4)	2.7219 (7)	171.79 (4)
Ow2—Hw22 $\cdots$ O21 <sup>vii</sup>	0.9568 (8)	1.9489 (4)	2.8544 (6)	157.09 (3)

Symmetry codes: (i)  $\frac{1}{2} + x, -\frac{1}{2} - y, 1 - z$ ; (ii)  $x, y - 1, z$ ; (iii)  $-x, y - \frac{1}{2}, \frac{3}{2} - z$ ; (iv)  $x - \frac{1}{2}, -\frac{1}{2} - y, 1 - z$ ; (v)  $-x, y - \frac{1}{2}, \frac{1}{2} - z$ ; (vi)  $x - \frac{1}{2}, \frac{1}{2} - y, 1 - z$ ; (vii)  $-x, \frac{1}{2} + y, \frac{3}{2} - z$ .

where the subscript  $m$  designates the multipole model and  $V$  is the unit-cell volume.

### 3. Results and discussion

#### 3.1. Crystal structure and molecular conformation

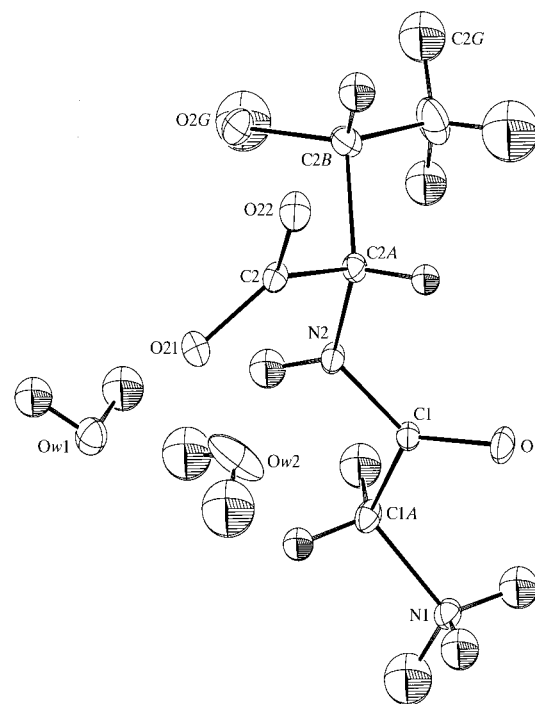
The  $a$  and  $c$  cell parameters decrease significantly during cooling (1.6%) and the relative variation of the unit cell volume is 3%. The molecular conformation is shown in Fig. 3(a). Bond distances, valence angles and torsion angles are given in Tables 4 and 5, respectively. Contrary to the results of Yadava & Padmanabhan (1973), the carboxylate group is clearly non-protonated [C—O21 1.2655 (6) and C2—O22 1.2459 (6)  $\text{\AA}$ ]. Nine hydrogen bonds occur in the GlyThr packing, as listed in Table 6. Each hydrogen of the amine group is involved in one hydrogen bond, one with the carboxylate group and the two others with solvent water molecules. The O21 atom of the carboxylate group takes part in three hydrogen bonds, whereas O22 takes part in only two hydrogen bonds. The crystal packing is shown in Fig. 3(b).

#### 3.2. Electron density

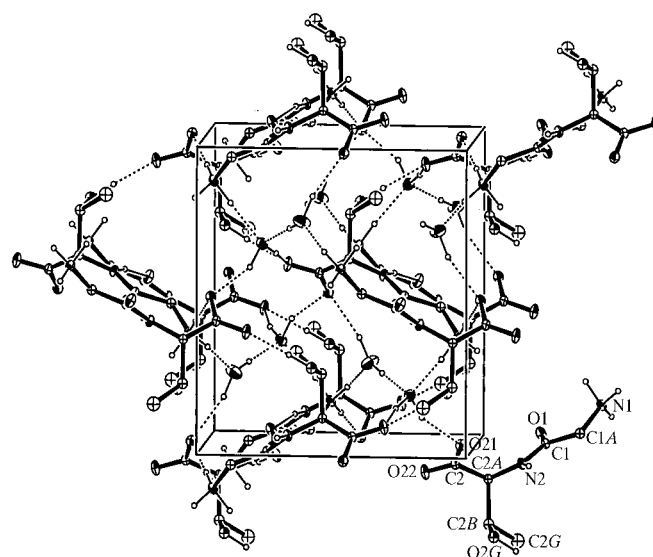
The experimental deformation electron density is calculated from

$$\Delta\rho(\mathbf{r}) = (1/V)\Sigma[|F_o| \exp(i\varphi_m) - |F_s| \exp(i\varphi_s)] \exp(-2\pi i\mathbf{H}\cdot\mathbf{r}) \quad (4)$$

where  $F_o$  and  $F_s$  are observed and spherical (IAM, independent atom model) structure-factor amplitudes;  $\varphi_m$  and  $\varphi_s$  are the multipolar and spherical phases, respectively. The sum is over structure factors [ $I > 3\sigma(I)$ ] to a resolution of  $(\sin \theta/\lambda)_{\max} = 0.9 \text{ \AA}^{-1}$ . The result of the experimental defor-



(a)

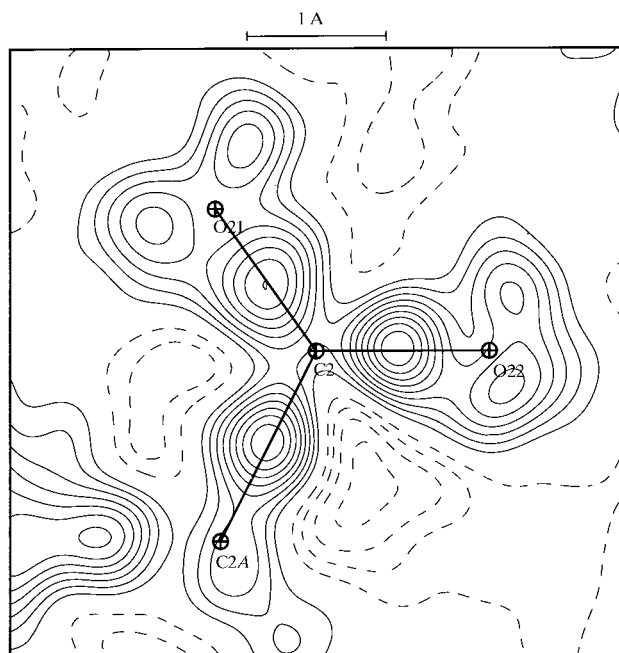


(b)

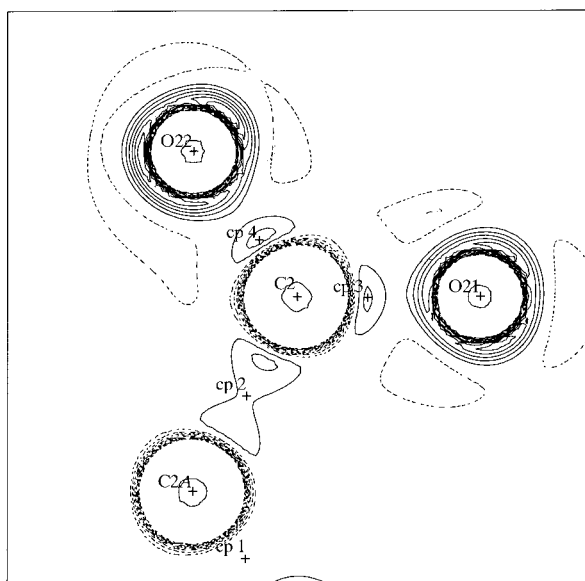
**Figure 3**  
(a) ORTEP view (Burnett & Johnson, 1996) of the asymmetric unit in GlyThr.2H<sub>2</sub>O. (b) Crystal packing and hydrogen bonds. Thermal ellipsoids are at the 50% probability level.

mation density in the peptide plane (C1, O1, N2) agrees quantitatively with our previous X-ray diffraction studies.

The experimental deformation map for the carboxylate group ( $\text{COO}^-$ ) is shown in Fig. 4(a); the O-atom lone pairs show up clearly, their heights vary in the range 0.25–0.30  $\text{e} \text{ \AA}^{-3}$  for O22 and reach 0.25  $\text{e} \text{ \AA}^{-3}$  for O21. The deformation density maxima are located on the covalent bonds and their maxima are 0.40  $\text{e} \text{ \AA}^{-3}$  for C2–O21 [1.2655 (6)  $\text{\AA}$ ] and 0.45  $\text{e} \text{ \AA}^{-3}$  for C2–O22 [1.2459 (6)  $\text{\AA}$ ], this is correlated with the length of the two C–O bonds. Also, very good agreement



(a)

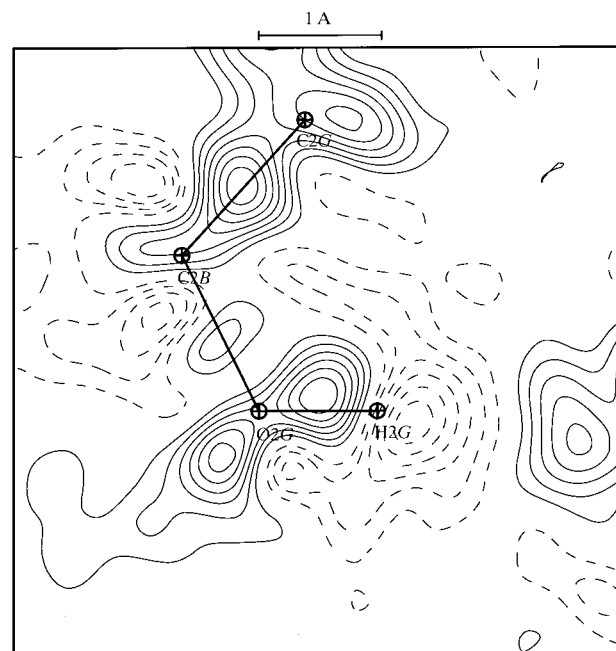


(b)

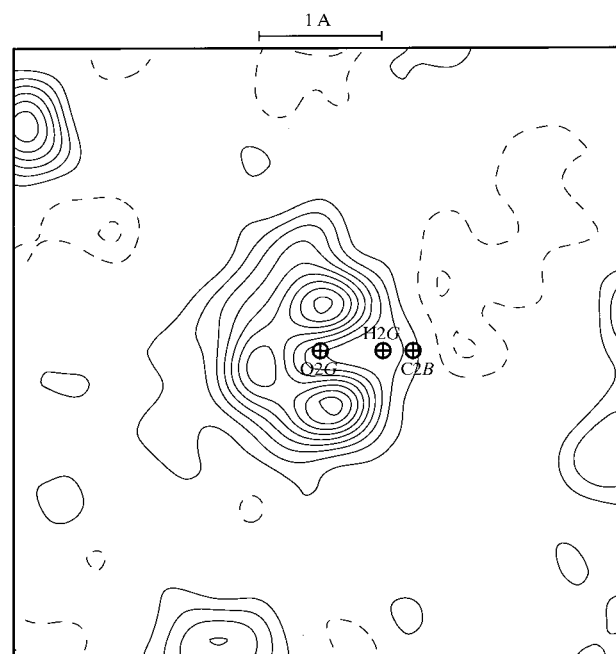
**Figure 4**  
(a) Experimental deformation electron density and (b) Laplacian of the electron density in the carboxylate group plane C2, O22 and O21. The label 'cp' on Fig. 4(b) denotes the critical point. Contours as in Fig. 2 and contour intervals for Laplacian are at 10  $\text{e} \text{ \AA}^{-5}$ .

within estimated errors (0.04  $\text{e} \text{ \AA}^{-3}$ ) is observed with our previous results for Leu-enkephalin trihydrate (Enk; Wiest *et al.*, 1994), *N*-acetyl-L-tryptophan methylamide (AcTr; Souhassou *et al.*, 1991) and L-cystine (Dahaoui, Pichon-Pesme *et al.*, 1999).

Fig. 5(a) gives the experimental deformation density map of the hydroxyl group in the COH plane (C2B, O2G, H2G). The deformation density maximum for the C–O bond [ $d =$



(a)



(b)

**Figure 5**  
(a) Experimental deformation electron density in the O2G, H2G and C2B plane; (b) in the plane bisecting O2G, H2G and C2B. Contours as in Fig. 2.

Table 7

Topological characteristics of electron density at the covalent bond critical points in GlyThr.

$\rho$  and  $\nabla^2\rho$  denote the electron density and its Laplacian at the critical point (CP).  $\lambda_1$ ,  $\lambda_2$  and  $\lambda_3$  are the eigenvalues of the Hessian of  $\rho$ .  $d_1$  and  $d_2$  are the distances from the CP to the first and the second atom defining the bond, respectively.  $d$  is the bond length. The average standard uncertainties of the position of critical point and the density at this critical point are estimated to be  $5 \times 10^{-3}$  Å,  $0.05 \text{ e } \text{Å}^{-3}$ , respectively. We estimate the standard uncertainty on the second derivatives of electron density ( $\rho$ ,  $\lambda$ ) to be 10% of their values (see Espinosa, Souhassou *et al.*, 1999).

	$d$ (Å)	$d_1$ (Å)	$d_2$ (Å)	$\rho$ ( $\text{e } \text{Å}^{-3}$ )	$\lambda_1, \lambda_2, \lambda_3$ ( $\text{e } \text{Å}^{-5}$ )	$\nabla^2\rho$ ( $\text{e } \text{Å}^{-5}$ )
C1—O1	1.232	0.492	0.740	2.75	6.7	−28.0
C2—O22	1.246	0.476	0.770	2.71	−23.9, −21.6, 21.8	−23.8
C2—O21	1.266	0.485	0.781	2.59	−21.8, −20.8, 20.4	−22.2
C2B—O2G	1.431	0.597	0.837	1.66	−11.8, −11.3, 17.0	−6.2
C1—N2	1.339	0.561	0.778	2.39	−22.9, −16.1, 16.7	−22.4
C2A—N2	1.447	0.610	0.838	1.70	−11.8, −10.3, 16.6	−5.6
C1A—N1	1.471	0.624	0.848	1.62	−12.0, −9.4, 14.7	−6.8
C2G—C2B	1.515	0.754	0.762	1.67	−10.9, −10.8, 11.7	−10.0
C1A—C1	1.516	0.744	0.772	1.74	−26.2, −23.0, 21.2	−14.4
C2A—C2	1.534	0.760	0.778	1.57	−11.2, −9.3, 9.8	−10.6
C2A—C2B	1.538	0.753	0.785	1.65	−10.7, −10.4, 10.9	−10.2
H2G—O2G	0.966	0.174	0.792	2.02	−37.7, −36.1, 25.8	−48.0
Hw11—Ow1	0.959	0.203	0.759	2.35	−37.4, −36.1, 25.8	−42.4
Hw12—Ow1	0.961	0.207	0.752	2.27		−41.7
Hw21—Ow2	0.954	0.213	0.740	2.32	−36.0, −34.2, 34.7	−35.6
Hw22—Ow2	0.957	0.215	0.741	2.32	−36.3, −33.9, 34.8	−35.3
HN2—N2	1.031	0.267	0.765	1.99	−25.5, −23.8, 23.0	−26.2
HN11—N1	1.034	0.238	0.797	1.84	−24.1, −23.6, 23.9	−23.8
HN12—N1	1.032	0.233	0.800	1.78	−24.5, −23.5, 23.8	−24.2
HN13—N1	1.033	0.230	0.802	1.83	−25.3, −24.7, 24.0	−26.1
H2A—C2A	1.083	0.377	0.706	1.70	−14.4, −13.9, 14.8	−13.5
H2B—C2B	1.088	0.318	0.771	1.70	−17.3, −16.3, 17.0	−16.6
H1A1—C1A	1.086	0.356	0.731	1.74	−16.4, −15.3, 14.7	−17.0
H1A2—C1A	1.087	0.372	0.720	1.67	−14.8, −13.8, 14.6	−14.0
H2G1—C2G	1.093	0.348	0.747	1.67	−15.7, −14.7, 17.4	−13.0
H2G2—C2G	1.081	0.396	0.686	1.64	−14.4, −12.4, 14.1	−12.8
H2G3—C2G	1.085	0.343	0.742	1.61	−15.4, −14.1, 17.3	−12.2

1.4314 (6) Å] is  $0.10 \text{ e } \text{Å}^{-3}$ . This is less pronounced than that obtained for the tyrosine C—O bond in L-tyrosyl-glycyl-glycine dihydrate (YGG; Pichon-Pesme *et al.*, 2000),  $0.40 \text{ e } \text{Å}^{-3}$  for  $d = 1.3701$  (9) Å, in Enk [ $0.20 \text{ e } \text{Å}^{-3}$  for  $d = 1.3596$  (9) Å] and in N-acetyl-L-tyrosine ethyl ester monohydrate (AcTyr; Dahaoui, Jelsch *et al.*, 1999),  $0.25 \text{ e } \text{Å}^{-3}$  for  $d = 1.3697$  (7) Å. In the bisecting plane of O2G, H2G and C2B (Fig. 5*b*), the lone pairs of O2G are very well resolved and their heights are  $0.40 \text{ e } \text{Å}^{-3}$ .

### 3.3. Topology of the electron density

A topological analysis (Bader, 1990) of the experimental electron density was carried out using the *NEWPROP* program (Souhassou, 1997; Souhassou & Blessing, 1999). The (3, −1) critical points that characterize the covalent bonding in the present crystal structure of GlyThr are listed in Table 7. In the heteronuclear C—N and C—O bonds, the bond critical point lies significantly closer to the C atom, in accordance with a greater accumulation of density concentrated in the more electronegative N or O atom (Fig. 4*b*). In the homonuclear C—C bonds, the bond critical point is approximately centered

between the two C atoms. The difference in  $\pi$  character of both C—O and C—N bonds is illustrated by the change in the properties of the bond critical point: for each bond type the values of density and the negative Laplacian at the critical point increase with the  $\pi$  character. These correlations between the properties of the critical points and the  $\pi$  character observed for GlyThr do not show up so clearly in Table 8, which is a compilation of experimental topological properties of C—O bonds, especially for the  $\lambda_i$  curvatures and Laplacian. These latter quantities are second derivatives and are more difficult to evaluate numerically when the interatomic distances are short or when the bond involves heavy atoms (Péres *et al.*, 1999). Then only  $\rho$ ,  $d_1$  and  $d_2$  may be accurately related to the strength of the bond.

For the covalent X—H bonds ( $X = \text{O, N, C}$ ) listed in Table 7, the Laplacian of  $\rho(\mathbf{r})$  increases as the X atom changes from C to N to O. It is also noteworthy that the four N—H covalent bonds have a very similar density and Laplacian at the critical point. We also observe that the critical point of the hydrogen bonds (Table 9) all lie in regions in which the Laplacian of the experimental density is positive, a characteristic of closed-shell interactions (Bader, 1990) which are governed by the contraction of the charge density towards each of the inter-

**Table 8**

Comparison of topological parameters for several C—O types in different compounds.

Symbols as in Table 7.

Bond	Compound	$d$ (Å)	$d_1$ (Å)	$d_2$ (Å)	$\rho$ (e Å <sup>-3</sup> )	$\lambda_1, \lambda_2, \lambda_3$ (e Å <sup>-5</sup> )	$\nabla^2\rho$ (e Å <sup>-5</sup> )	
C=O	GlyThr	1.232	0.493	0.740	2.75	-26.2, -23.0, 21.2	-28.0	
		YGG (Lachekar, 1997)	1.223	0.453	0.769	2.79	-23.8, -21.6, 27.5	-17.8
	GD (Lachekar, 1997)	1.242	0.475	0.766	2.71	-22.7, -21.3, 21.4	-22.6	
		1.233	0.460	0.773	2.59	-21.9, -20.2, 26.3	-15.8	
		Enk (Wiest <i>et al.</i> , 1994)	1.242	0.459	0.777	2.93	-28.6, -26.7, 23.9	-31.4
		1.249	0.463	0.779	2.91	-28.2, -26.2, 22.5	-31.9	
		1.251	0.462	0.779	2.92	-28.3, -26.4, 22.9	-31.8	
		AcTr (Souhassou <i>et al.</i> , 1991)	1.232	0.485	0.748	2.81	-24.0, -21.2, 23.1	-21.0
	AcTyr (Dahaoui, Jelsch <i>et al.</i> , 1999)	1.248	0.498	0.750	2.74	-23.1, -21.2, 23.1	-21.2	
		1.240	0.485	0.755	2.88	-26.0, -23.5, 20.1	-29.4	
	C=O (COOH)	GD (Lachekar, 1997)	1.216	0.453	0.763	2.78	-26.6, -22.6, 26.2	-23.0
		D,L-Aspartic acid (Flaig <i>et al.</i> , 1998)	1.226		0.784	2.96		-42.2
C—O (COO)	GlyThr	1.246	0.476	0.770	2.71	-23.9, -21.7, 21.8	-23.8	
		1.266	0.485	0.781	2.59	-21.8, -20.8, 20.4	-22.2	
	YGG (Lachekar, 1997)	1.254	0.452	0.802	2.57	-22.0, -20.0, 28.5	-13.5	
		1.260	0.458	0.803	2.56	-21.3, -20.0, 26.0	-15.3	
	GD (Lachekar, 1997)	1.257	0.463	0.793	2.68	-24.1, -21.0, 23.4	-21.8	
		1.258	0.458	0.800	2.41	-20.7, -18.5, 27.0	-12.2	
	L-Alanine (Destro <i>et al.</i> , 1991)	1.248	0.517		3.02	-31.4, -26.4, 18.8	-39.5	
		1.267	0.540		2.86	-27.6, -24.4, 22.5	-29.5	
	LAP (Espinosa <i>et al.</i> , 1996)	1.245	0.494	0.751	2.68	-25.9, -21.7, 23.9	-23.7	
		1.269	0.514	0.755	2.59	-24.4, -20.4, 21.9	-23.7	
	D,L-Aspartic acid (Flaig <i>et al.</i> , 1998)	1.255		0.763	2.87		-36.1	
		1.262		0.800	2.71		-37.6	
		1.255	0.442	0.815	2.55	-22.7, -21.8, 30.7	-13.8	
	Enk (Wiest <i>et al.</i> , 1994)	1.262	0.444	0.820	2.39	-20.3, -20.0, 30.5	-9.8	
		1.317	0.512	0.805	2.38	-21.9, -17.1, 16.8	-22.1	
C—OH (COOH)	GD (Lachekar, 1997)	1.313		0.803	2.41		-29.7	
	D,L-Aspartic acid (Flaig <i>et al.</i> , 1998)	1.313		0.803	2.41		-29.7	
C(ring)—OH	YGG (Lachekar, 1997)	1.370	0.598	0.793	1.83	-12.7, -10.2, 20.6	-2.3	
	AcTyr (Dahaoui, Jelsch <i>et al.</i> , 1999)	1.370	0.559	0.811	1.96	-16.0, -15.0, 19.0	-12.0	
	Enk (Wiest <i>et al.</i> , 1994)	1.360	0.593	0.767	2.12	-16.2, -15.8, 17.1	-14.8	
Csp <sup>3</sup> —OH	GlyThr	1.431	0.597	0.837	1.66	-11.8, -11.3, 17.0	-6.2	

**Table 9**

Topological characteristics of the electron density at the hydrogen-bond critical points in GlyThr.

Symbols as in Table 7.  $G_c$  and  $G_{\text{exp}}$  are, respectively, the evaluation of the kinetic energy density for closed-shell interactions at the critical point as proposed by Abramov (1997) and by Espinosa, Lecomte & Molins (1999).

Bond	$d$ (Å)	$d_1$ (Å)	$d_2$ (Å)	$\rho$ (e Å <sup>-3</sup> )	$\lambda_1, \lambda_2, \lambda_3$ (e Å <sup>-5</sup> )	$\nabla^2$ (e Å <sup>-5</sup> )	$G_{\text{exp}}$ (a.u.)	$G_c$ (a.u.)
HN12...Ow2	1.654	0.522	1.135	0.22	-1.4, -1.3, 8.1	5.4	0.0472	0.0476
Hw12...O22	1.766	0.616	1.189	0.17	-0.9, -0.8, 5.6	3.9	0.0326	0.0332
Hw21...Ow1	1.775	0.588	1.191	0.16	-0.8, -0.7, 6.1	4.6	0.0355	0.0374
HN11...O21	1.779	0.604	1.188	0.22	-1.1, -1.1, 5.6	3.4	0.0326	0.0331
H2G...O22	1.795	0.577	1.219	0.13	-0.5, -0.5, 5.2	3.6	0.0303	0.0275
HN13...Ow1	1.818	0.717	1.270	0.14	-0.8, -0.6, 2.4	2.4	0.0140	0.0211
Hw11...O21	1.838	0.604	1.188	0.22	-1.1, -1.0, 5.2	3.4	0.0303	0.0331
Hw22...O21	1.950	0.685	1.287	0.11	-0.6, -0.4, 4.0	2.9	0.0233	0.0231
HN2...O1	1.974	0.695	1.307	0.08	-0.3, -0.3, 3.0	2.4	0.0175	0.0184

acting nuclei. Indeed, we find that the  $\lambda_3$  curvature of the density in the direction along the bond path is dominant; in earlier papers (Espinosa *et al.*, 1998; Espinosa, Lecomte & Molins, 1999; Espinosa, Souhassou *et al.*, 1999), we have studied the relationship between the energetic properties of the hydrogen-bond interaction and the topological overlapping of the electronic clouds at the H...O critical point.

One of the most interesting results is the linear correlation between the  $\lambda_3$  curvature and the kinetic energy density  $G$  at the critical point:  $G = a\lambda_3$ , where  $a = 15.3 \text{ Å}^5 \text{ kJ e}^{-1} \text{ mol}^{-1}$  (Espinosa, Lecomte & Molins, 1999). The values obtained by this formula and those calculated using the Abramov functional (Abramov, 1997) are in very good agreement for all hydrogen bonds in GlyThr (Table 9).

### 3.4. Net atomic charges and dipole moments

Table 10 gives the net charges obtained from the kappa refinement (refinement  $E$  in Table 2). The net charges of the  $\text{COO}^-$  and  $\text{NH}_3^+$  groups obtained are  $-0.52 e$  and  $+0.31 e$ ,

respectively, by comparison to those found in the same groups of Enk ( $-0.88$  and  $+0.88 e$ ); L-arginine phosphate (LAP; Espinosa *et al.*, 1996),  $-0.67$  and  $+0.57 e$ ; L-glycyl-aspartic acid monohydrate (GD; Lachekar, 1997),  $-0.66$  and  $+0.48 e$ ; YGG,  $-0.37$  and  $+0.40 e$ . As observed in previous studies, the

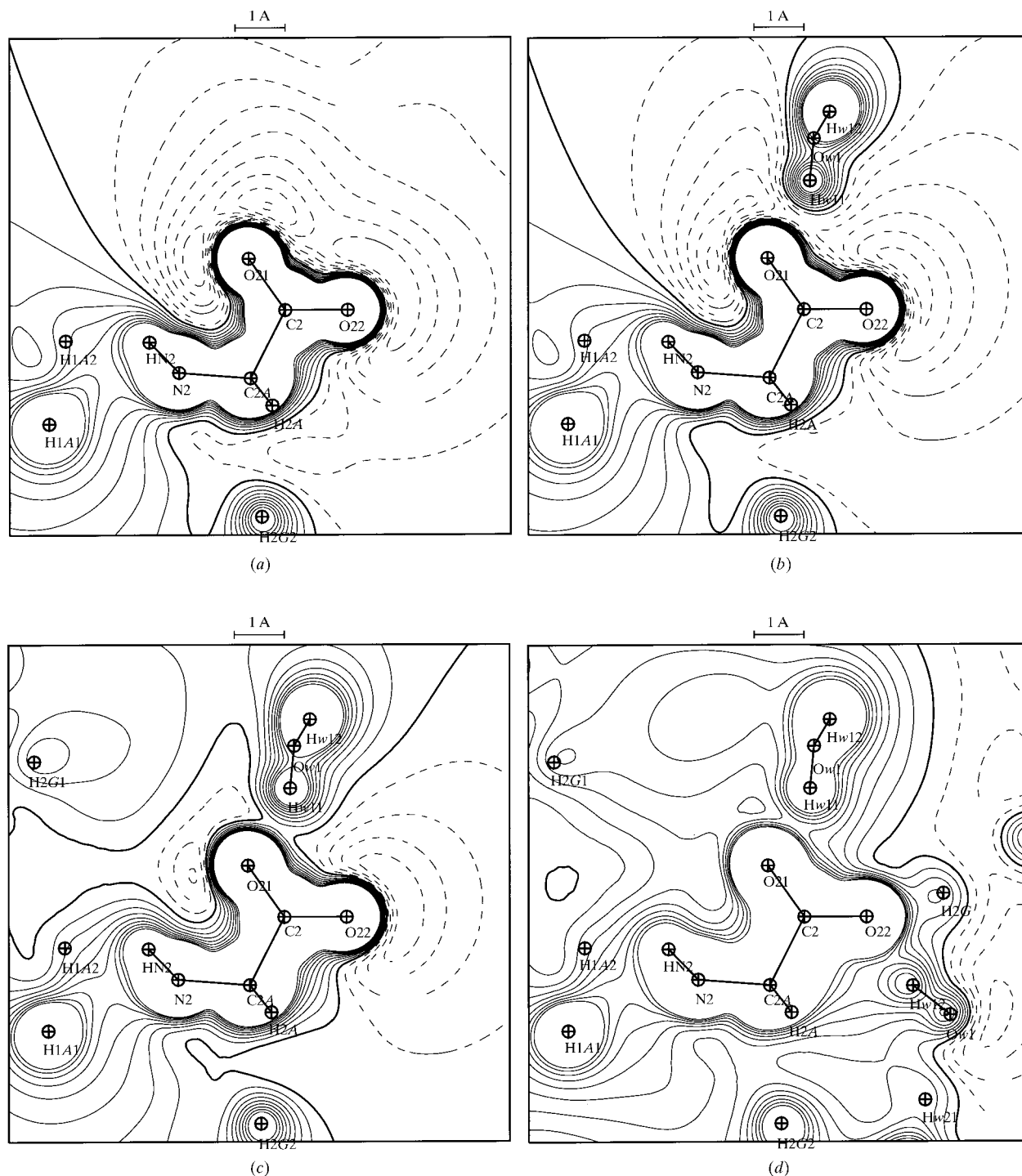


**Figure 6**

Electrostatic potential in the C2, O22 and O21 carboxylate group plane generated by: (a) one pseudo-isolated GlyThr molecule; (b) GlyThr and one water molecule *via* the hydrogen bond  $\text{O21} \cdots \text{Hw11}$ ; (c) GlyThr with two interacting molecules (one GlyThr *via* hydrogen bonds  $\text{O21} \cdots \text{HN11}$  and one water molecule); (d) GlyThr with all hydrogen bonds. Contour intervals are at  $0.05 e \text{ \AA}^{-1}$ ; solid lines represent positive contours, dashed lines negative contours and thick solid lines zero contours.

**Table 10**

Net atomic charge ( $e$ ) and kappa parameter after refinement  $E$  (Table 2).

The standard uncertainties are given in parentheses.

	$q$	$\kappa$		$q$	$\kappa$
C1A	-0.12 (4)	1.029 (6)	HN11	0.33 (2)	1.33 (3)
C1	0.22 (4)	1.051 (6)	HN12	0.38 (3)	1.23 (3)
C2A	-0.17 (4)	1.032 (6)	HN13	0.32 (2)	1.33 (3)
C2B	0.02 (4)	1.037 (6)	H2A	0.08 (2)	1.30 (2)
C2G	-0.66 (5)	1.013 (5)	H2G1	0.32 (3)	1.35 (4)
C2	0.23 (4)	1.054 (6)	H2G2	0.27 (3)	1.29 (3)
			H2G3	0.23 (3)	1.32 (3)
N1	-0.72 (3)	0.990 (4)	H1A1	0.28 (3)	1.26 (3)
N2	-0.53 (4)	1.001 (3)	H1A2	0.24 (2)	1.26 (3)
			HN2	0.36 (2)	1.35 (3)
O1	-0.34 (3)	0.987 (3)	H2B	0.09 (3)	1.20 (2)
O2G	-0.34 (3)	0.984 (3)	H2G	0.32 (3)	1.09 (3)
O21	-0.39 (3)	0.991 (3)			
O22	-0.36 (3)	0.990 (3)	Hw11	0.24 (2)	1.29 (3)
			Hw12	0.28 (2)	1.30 (3)
Ow1	-0.52 (2)	0.977 (3)	Hw21	0.29 (2)	1.17 (4)
Ow2	-0.56 (3)	0.987 (3)	Hw22	0.28 (2)	1.23 (4)

CONH peptide moiety is not neutral but bears a negative charge ( $-0.29 e$ ) compared with  $-0.46 e$  in Enk and  $-0.40$  in YGG.

The dipole moment (Espinosa *et al.*, 1996) calculated from the kappa and multipolar refinement, are 19.9 (1.2) and 23.8 (3.8) D, respectively, with the main contribution from the charged groups  $\text{COO}^-$  and  $\text{NH}_3^+$ . By comparison, the dipole moment, calculated from the multipolar refinement of Enk is 55.2 D.

For the two solvent water molecules, the dipole moments are 1.5 (0.1) and 1.8 (0.1) D after kappa refinement  $E$ , and 1.6 (0.3) and 2.2 (0.8) D after multipolar refinement  $D$ , which compares well with the average experimental values given by Bouhmaida *et al.* (1999),  $\langle \mu \rangle = 2.20$  D.

### 3.5. Electrostatic potential

We have calculated the electrostatic potential around the GlyThr molecule in direct space using the *ELECTROS* program (Ghermani *et al.*, 1992) for parameters of refinement  $D$ , in order to characterize the potential of the  $\text{COO}^-$  group as a hydrogen-bond acceptor. As described above, this carboxylate group accepts five hydrogen bonds, three of them involving C2–O21 (Table 6).

Fig. 6(a) displays the electrostatic potential generated around the carboxylate group in the C2, O22 and O21 plane by an isolated molecule of GlyThr (*i.e.* removed from the crystal lattice). We obtain a very negative and slightly asymmetric potential. This electrostatic potential is very extended owing to the additive effect of the two O atoms, as their respective negative charges are  $-0.33$  and  $-0.23 e$ . In Fig. 6(b), one GlyThr molecule and one water molecule interact *via* the intramolecular hydrogen bond [O21–Hw11 1.8384 (4) Å]: the deep negative region around the O21 atom is divided into two parts on each side of the Hw11–O21 hydrogen bond, but the depth of the potential did not decrease. Then, the electrostatic potential generated by O21

and its two interacting molecules (two GlyThr and one water molecule) *via* hydrogen bonds O21–HN11 1.7915 (4) Å ( $x - \frac{1}{2}, -y - \frac{1}{2}, -z + 1$ ) and O21–Hw11, respectively, is given in Fig. 6(c). At this stage, the negative potential around the O21 oxygen has been totally neutralized and a valley of positive potential is formed. The potential minimum close to O22 decreases from  $0.05 e \text{ \AA}^{-1}$  only allowing other hydrogen-bond interactions with O22 as a donor. Finally, we have calculated the electrostatic potential generated by all the interacting molecules *via* hydrogen bonds (Fig. 6d). The negative potential around the carboxylate group has been entirely neutralized and the potential is almost positive everywhere.

### 4. Conclusions

This investigation has provided detailed information about the electron distribution in GlyThr. A full quantitative characterization of all interatomic interactions has been obtained through the topological analysis of  $\rho$  and the effect of hydrogen bonds on the electrostatic potential has been analyzed.

### References

- Abramov, Yu. A. (1997). *Acta Cryst.* **A53**, 264–272.  
 Allen, F. H. (1986). *Acta Cryst.* **B42**, 515–522.  
 Bader, R. F. W. (1990). *Atoms in Molecules: A Quantum Theory*. The International Series of Monographs of Chemistry, edited by J. Halpen and M. L. H. Green. Oxford: Clarendon Press.  
 Blessing, R. H. (1987). *Crystallogr. Rev.* **1**, 3–58.  
 Blessing, R. H. (1989). *J. Appl. Cryst.* **22**, 396–397.  
 Bouhmaida, N., Ghermani, N.-E., Lecomte, C. & Thallal, A. (1999). *Acta Cryst.* **A55**, 729–738.  
 Burnett, M. N. & Johnson, C. K. (1996). *ORTEP III*. (1996). *Thermal Ellipsoid Plot Program for Crystal Structure Illustrations*. Report ORNL-6895. Oak Ridge National Laboratory, Tennessee, USA.  
 Clementi, E. & Raimondi, D. L. (1963). *J. Chem. Phys.* **41**, 2686–2689.  
 Coppens, P., Gern, T. N., Lung, P., Stevens, E. D., Becker, P. & Yang, Y. N. (1979). *Acta Cryst.* **A35**, 63–79.  
 Cromer, D. T. (1974). *International Tables for X-ray Crystallography*, edited by J. A. Ibers and W. E. Hamilton, pp. 148–151. Birmingham: Kynoch Press.  
 Cruickshank, D. W. J. (1949). *Acta Cryst.* **2**, 65–82.  
 Dahaoui, S., Jelsch, C., Howard, J. A. K. & Lecomte, C. (1999). *Acta Cryst.* **B55**, 226–230.  
 Dahaoui, S., Pichon-Pesme, V., Howard, J. A. K. & Lecomte, C. (1999). *J. Phys. Chem. A*, **103**, 6240–6250.  
 Destro, R., Bianchi, R., Gatti, C. & Merati, F. (1991). *Chem. Phys. Lett.* **186**, 47–52.  
 Enraf–Nonius (1989). *CAD-4 Software*. Enraf–Nonius, Delft, The Netherlands.  
 Espinosa, E., Lecomte, C. & Molins, E. (1999). *Chem. Phys. Lett.* **300**, 745–748.  
 Espinosa, E., Lecomte, C., Molins, E., Veintemillas, S., Cousson, A. & Paulus, W. (1996). *Acta Cryst.* **B52**, 519–534.  
 Espinosa, E., Molins, E. & Lecomte, C. (1998). *Chem. Phys. Lett.* **285**, 170–173.  
 Espinosa, E., Souhassou, M., Lachekar, H. & Lecomte, C. (1999). *Acta Cryst.* **B55**, 563–572.  
 Flaig, R., Koritsanszky, T., Zobel, D. & Luger, P. (1998). *J. Am. Chem. Soc.* **120**, 2227–2238.

- Ghermani, N.-E., Bouhaida, N. & Lecomte, C. (1992). *ELECTROS. Computer Program to Calculate Electrostatic Properties from High Resolution X-ray Diffraction*. Internal reports URA CNRS 809, University of Nancy 1, France.
- Hansen, N. K. & Coppens, P. (1978). *Acta Cryst.* **A34**, 909–921.
- Hirshfeld, F. L. (1976). *Acta Cryst.* **A32**, 239–244.
- Housset, D., Benabicha, F., Pichon-Pesme, V., Jelsch, C., Maierhofer, A., David, S., Fontecilla-Camps, J. C. & Lecomte, C. (2000). *Acta Cryst.* **D56**. In the press.
- Jelsch, C., Pichon-Pesme, V., Lecomte, C. & Aubry, A. (1998). *Acta Cryst.* **D54**, 1306–1318.
- Lachekar, H. (1997). PhD thesis. Université of Henri Poincaré-Nancy 1, France.
- Pérès, N., Boukhris, A., Souhassou, M., Gavaille, G. & Lecomte, C. (1999). *Acta Cryst.* **A55**, 1038–1048.
- Pichon-Pesme, V., Lachekar, H., Souhassou, M. & Lecomte, C. (2000). *Acta Cryst.* Submitted.
- Pichon-Pesme, V. & Lecomte, C. (1998). *Acta Cryst.* **B54**, 485–493.
- Pichon-Pesme, V., Lecomte, C. & Lachekar, H. (1995). *J. Phys. Chem.* **99**, 6242–6250.
- Pichon-Pesme, V., Lecomte, C., Wiest, R. & Bénard, M. (1992). *J. Am. Chem. Soc.* **114**, 2713–2715.
- Rees, B. (1976). *Acta Cryst.* **A32**, 483–488.
- Souhassou, M. (1997). *NEWPROP. Computer Program to Calculate the Topological Properties of Electron Density*. Internal Report CNRS ESA 7036, UAP, Nancy, France.
- Souhassou, M. & Blessing, R. H. (1999). *J. Appl. Cryst.* **32**, 210–217.
- Souhassou, M., Lecomte, C., Blessing, R. H. & Aubry, A., Rohmer, M.-M., Wiest, R. & Bénard, M. (1991). *Acta Cryst.* **B47**, 253–266.
- Souhassou, M., Lecomte, C., Ghermani, N.-E., Rohmer, M.-M., Wiest, R., Bénard, M. & Blessing, R. H. (1992). *J. Am. Chem. Soc.* **114**, 2371–2382.
- Sheldrick, G. M. (1990). *Acta Cryst.* **A46**, 467–473.
- Sheldrick, G. M. (1993). *SHELXL93. Program for the Refinement of Crystal Structures*. University of Göttingen, Germany.
- Stewart, R. F., Davidson, E. R. & Simpson, W. T. (1965). *J. Chem. Phys.* **43**, 175–187.
- Wiest, R., Pichon-Pesme, V., Bénard, M. & Lecomte, C. (1994). *J. Phys. Chem.* **98**, 1351–1362.
- Yadava, V. S. & Padmanabhan, V. M. (1973). *Acta Cryst.* **B29**, 854–858.